

Phonon Decoherence of a Double Quantum Dot Charge Qubit

Serguei Vorotsov,¹ Eduardo R. Mucciolo,^{2,3} and Harold U. Baranger¹

¹*Department of Physics, Duke University, Box 90305, Durham, North Carolina 27708-0305*

²*Department of Physics, University of Central Florida, Box 162385, Orlando, Florida 32816-2385*

³*Departamento de Física, Pontifícia Universidade Católica do Rio de Janeiro, C.P. 37801, 22452-970 Rio de Janeiro, Brazil*

(Dated: March 23, 2022)

We study decoherence of a quantum dot charge qubit due to coupling to piezoelectric acoustic phonons in the Born-Markov approximation. After including appropriate form factors, we find that phonon decoherence rates are one to two orders of magnitude weaker than was previously predicted. We calculate the dependence of the Q -factor on lattice temperature, quantum dot size, and interdot coupling. Our results suggest that mechanisms other than phonon decoherence play a more significant role in current experimental setups.

PACS numbers: 03.67.Lx, 73.21.La, 71.38.-k

Keywords: quantum computation, quantum dots, qubits, decoherence, phonons

I. INTRODUCTION

Since the discovery that quantum algorithms can solve certain computational problems much more efficiently than classical ones,¹ attention has been devoted to the physical implementation of quantum computation. Among the many proposals, there are those based on the electron spin^{2,3} or charge^{4,5,6,7,8} in laterally confined quantum dots, which may have great potential for scalability and integration within current technologies.

Single qubit operations involving the spin of an electron in a quantum dot will likely require precise engineering of the underlying material or control over local magnetic fields;⁹ both have yet to be achieved in practice. In contrast, single qubit operations involving charge in a double quantum dot (DQD)¹⁰ are already within experimental reach.^{11,12} They can be performed either by sending electrical pulses to modulate the potential barrier between the dots (tunnel pulsing)^{6,8} or by changing the relative position of the energy levels (bias pulsing).¹¹ In both cases one acts on the overlap between the electronic wave functions of the dots. This permits direct control over the two low-energy charge states of the system – the basis states $|1\rangle$ and $|2\rangle$ of a qubit: Calling N_1 (N_2) the number of excess electrons in the left (right) dot, we have that $|1\rangle = (1, 0)$ and $|2\rangle = (0, 1)$.

The proposed DQD charge qubit relies on having two lateral quantum dots tuned to the $(1, 0) \leftrightarrow (0, 1)$ transition line of the Coulomb blockade stability diagram (see Fig. 1). Along this line, an electron can move between the dots with no charging energy cost. An advantage of this system is that the Hilbert space is two-dimensional, even at moderate temperatures, since single-particle excitations do not alter the charge configuration. Leakage from the computational space involves energies of order the charging energy which is quite large in practice (~ 1 meV ~ 10 K). In the case of tunnel pulsing, working adiabatically – such that the inverse of the switching time is much less than the charging energy – assures minimal leakage. The large charging energy implies that pulses as short as tens to hundreds of picoseconds would be well within the adiabatic regime. However, the drawback of using charge to build qubits is the high decoherence rates when compared to spin. Since for any successful qubit one must be able to

perform single- and double-qubit operations much faster than the decoherence time, a quantitative understanding of decoherence mechanisms in a DQD is essential.

In this work, we carry out an analysis of phonon decoherence in a DQD charge qubit. During qubit operations, the electron charge movement induces phonon creation and annihilation, thus leading to energy relaxation and decoherence. In order to quantify these effects, we follow the time dependence of the system's reduced density matrix, after tracing out the phonon bath, using the Redfield formalism in the Born and Markov approximations.^{13,14}

Our results show that decoherence rates for this situation are one to two orders of magnitude weaker than previously estimated. The discrepancy arises mainly due to the use of different spectral functions. Our model incorporates realistic geometric features which were lacking in previous calculations. When compared to recent experimental results, our calculations indicate that phonons are likely not the main source of decoherence in current DQD setups.

The paper is organized as follows. In Sec. II, we introduce the model used to describe the DQD, discuss the coupling to phonons, and establish the Markov formulation used to solve for the reduced density matrix. In Sec. III we study decoherence in a single-qubit operation, while in Sec. IV we simulate

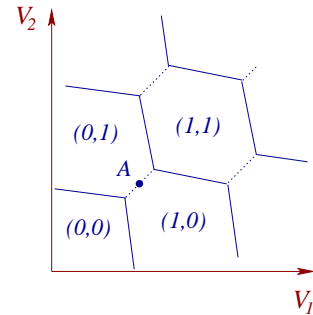


FIG. 1: Schematic Coulomb blockade stability diagram for a double quantum dot system at zero bias.¹⁰ (N_1, N_2) denotes the number of excess electrons in the dots for given values of the gate voltages V_1 and V_2 . The solid lines indicate transitions in the total charge, while the dotted lines indicate transitions where charge only moves between dots. The point A marks the qubit working point.

the bias pulsing experiment of Ref. 11. Finally, in Sec. V we present our conclusions.

II. MODEL SYSTEM

We begin by assuming that the DQD is isolated from the leads. The DQD and the phonon bath combined can then be described by the total Hamiltonian⁷

$$H = H_S + H_B + H_{SB}, \quad (1)$$

where H_S and H_B are individual DQD and phonon Hamiltonians, respectively, and H_{SB} is the electron-phonon interaction. We assume that gate voltages are tuned to bring the system near the degeneracy point A (Fig. 1) where a single electron may move between the two dots with little charging energy cost. To simplify the presentation, only one quantum level on each dot is included; $E_{1(2)}$ denotes the energy of an excess electron on the left (right) QD (possibly including some charging energy). Likewise, spin effects are neglected.¹⁵ Thus, in the basis $\{|1\rangle, |2\rangle\}$, the DQD Hamiltonian reads

$$H_S = \frac{\varepsilon(t)}{2} \sigma_z + v(t) \sigma_x, \quad (2)$$

where $\sigma_{z,x}$ are Pauli matrices, $\varepsilon(t) = E_1 - E_2$ is the energy level difference, and $v(t)$ is the tunneling amplitude connecting the dots. Notice that both ε and v may be time dependent. The phonon bath Hamiltonian has the usual form ($\hbar = 1$)

$$H_B = \sum_{\mathbf{q}} \omega_{\mathbf{q}} b_{\mathbf{q}}^\dagger b_{\mathbf{q}}, \quad (3)$$

where the dispersion relation $\omega_{\mathbf{q}}$ is specified below. The electron-phonon interaction has the linear coupling form,^{7,16}

$$H_{SB} = \sum_{\mathbf{q}} \sum_{i=1}^2 \alpha_{\mathbf{q}}^{(i)} N_i (b_{\mathbf{q}}^\dagger + b_{-\mathbf{q}}), \quad (4)$$

where N_i is the number of excess electrons in the i -th dot and $\alpha_{\mathbf{q}}^{(i)} = \lambda_{\mathbf{q}} e^{-i\mathbf{q} \cdot \mathbf{R}_i} P_i(\mathbf{q})$, with $\mathbf{R}_1 = 0$ and $\mathbf{R}_2 = \mathbf{d}$ the dot position vectors, see Fig. 2. The dependence of the coupling constant $\lambda_{\mathbf{q}}$ on the material parameters and on the wave vector \mathbf{q} will be specified below. The dot form factor is

$$P_i(\mathbf{q}) = \int d^3r n_i(\mathbf{r}) e^{-i\mathbf{q} \cdot \mathbf{r}}, \quad (5)$$

where $n_i(\mathbf{r})$ is the excess charge density in the i -th dot. With no significant loss of generality, we will assume that the form factor is identical for both dots and, therefore, drop the i index hereafter. In the basis $\{|1\rangle, |2\rangle\}$, after dropping irrelevant constant terms, the electron-phonon interaction simplifies to

$$H_{SB} = K \Phi, \quad (6)$$

where

$$K = \frac{1}{2} \sigma_z \quad \text{and} \quad \Phi = \sum_{\mathbf{q}} g_{\mathbf{q}} (b_{\mathbf{q}}^\dagger + b_{-\mathbf{q}}), \quad (7)$$

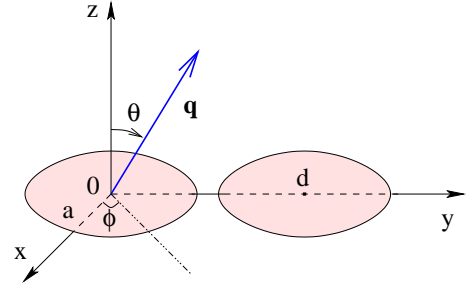


FIG. 2: Geometry of the double quantum dot charge qubit.

with $g_{\mathbf{q}} = \lambda_{\mathbf{q}} P(\mathbf{q}) (1 - e^{-i\mathbf{q} \cdot \mathbf{d}})$. The phonons propagate in three dimensions, while the electrons are confined to the plane of the underlying two-dimensional electron gas (2DEG). Notice that the electron-phonon coupling is not isotropic for the DQD (Fig. 2): Phonons propagating along $\phi = 0$ and any θ do not cause any relaxation, while coupling is maximal along $\phi = \theta = \pi/2$ direction. We neglect any mismatch in phonon velocities at the GaAs/AlGaAs interface, where the 2DEG is located.

We now proceed with the Born-Markov-Redfield treatment^{13,14} of this system. While the Born approximation is clearly justified for weak electron-phonon interaction, the Markov approximation requires, in addition, that the bath correlation time is the smallest time scale in the problem. These conditions are reasonably satisfied for lateral GaAs quantum dots, as we will argue below.

Let us assume that the system and the phonon bath are disentangled at $t = 0$. Using Eqs. (2), (3), and (6), we can write the Redfield equation for the reduced density matrix $\rho(t)$ of the DQD^{13,14},

$$\dot{\rho}(t) = -i[H_S(t), \rho(t)] + \{[\Lambda(t)\rho(t), K] + \text{H.c.}\}. \quad (8)$$

The first term on the right-hand side yields the Liouvillian evolution and the other terms yield the relaxation caused by the phonon bath. The auxiliary matrix Λ is defined as

$$\Lambda(t) = \int_0^\infty d\tau B(\tau) e^{-i\tau H_S(t)} K e^{i\tau H_S(t)} \quad (9)$$

where $B(\tau) = \text{Tr}_b\{\Phi(\tau)\Phi(0)f(H_B)\}$ is the bath correlation function, $\Phi(\tau) = e^{iH_B\tau}\Phi e^{-iH_B\tau}$, and $f(H_B) = e^{-\beta H_B}/\text{Tr}_b\{e^{-\beta H_B}\}$, with $\beta = 1/T$ the inverse lattice temperature ($k_B = 1$).

Using Eq. (3) in the definition of the bath correlation function, we find that the latter can be expressed in the form

$$B(\tau) = \int_0^\infty d\omega \nu(\omega) \{e^{i\tau\omega} n_B(\omega) + e^{-i\tau\omega} [1 + n_B(\omega)]\}, \quad (10)$$

where $n_B(\omega)$ is the Bose-Einstein distribution function and

$$\nu(\omega) = \sum_{\mathbf{q}} |g_{\mathbf{q}}|^2 \delta(\omega - \omega_{\mathbf{q}}) \quad (11)$$

is the spectral density of the phonon bath.

We now specialize to linear, isotropic acoustic phonons: $\omega_{\mathbf{q}} = s|\mathbf{q}|$, where s is the phonon velocity. Moreover, we

only consider coupling to longitudinal piezoelectric phonons, neglecting the deformation potential contribution. For bulk GaAs, this is justifiable at temperatures below approximately 10 K.¹⁷ Thus,

$$|\lambda_{\mathbf{q}}|^2 = \frac{g_{\text{ph}} \pi^2 s^2}{\Omega |\mathbf{q}|}, \quad (12)$$

where g_{ph} is the piezoelectric constant in dimensionless form ($g_{\text{ph}} \approx 0.05$ for GaAs^{16,17}) and Ω is the unit cell volume.

The excess charge distribution in the dots is assumed Gaussian:

$$n(\mathbf{r}) = \delta(z) \frac{1}{2\pi a^2} \exp\left(-\frac{x^2 + y^2}{2a^2}\right). \quad (13)$$

This is certainly a good approximation for small dots with few electrons, but becomes less accurate for large dots. The resulting form factor reads

$$P(\mathbf{q}) = e^{-(q_x^2 + q_y^2)a^2/2}. \quad (14)$$

Note that this expression differs from that in Refs. 6 and 8 where a three-dimensional Gaussian charge density was assumed.

Using Eqs. (12) and (14), as well as the DQD geometry of Fig. 2, we get

$$\begin{aligned} \nu(\omega) = g_{\text{ph}} \omega \int_0^{\pi/2} d\theta \sin \theta \exp\left(-\frac{\omega^2 a^2}{s^2} \sin^2 \theta\right) \\ \times \left[1 - J_0\left(\frac{\omega d}{s} \sin \theta\right)\right]. \end{aligned} \quad (15)$$

It is instructive to inspect the asymptotic limits of this equation. At low frequencies, $\nu(\omega \rightarrow 0) \approx g_{\text{ph}} d^2 \omega^3 / 6s^2$; thus, the phonon bath is superohmic. At high frequencies,

$$\nu(\omega \rightarrow \infty) \approx \frac{g_{\text{ph}} s^2}{a^2 \omega} f\left(\frac{d}{a}\right), \quad (16)$$

where

$$f\left(\frac{d}{a}\right) = \int_0^\infty dx x e^{-x^2} \left[1 - J_0\left(\frac{d}{a} x\right)\right]. \quad (17)$$

Notice that the spectral function does not have the exponential decay familiar from the spin-boson model, but rather falls off much more slowly: $\nu(\omega \rightarrow \infty) \propto \omega^{-1}$. This should be contrasted with the phenomenological expressions used in Ref. 7.

The characteristic frequency of the maximum in $\nu(\omega)$ is $\tau_c^{-1} = s/a$. For typical experimental setups, $a \approx 50$ nm while $s \approx 5 \times 10^3$ m/s for GaAs, yielding $\tau_c \approx 10$ ps ($\tau_c^{-1} \approx 65$ μeV). Thus, the Markovian approximation can be justified for time scales $t > \tau_c$ and if all pulse operations are kept adiabatic on the scale of τ_c .

III. DECAY OF CHARGE OSCILLATIONS

One can operate this charge qubit in two different ways: (i) by pulsing the tunneling amplitude $v(t)$ keeping ε constant,

or (ii) by changing the energy level difference $\varepsilon(t)$ keeping v constant (bias pulsing). Tunnel pulsing seems advantageous as it implies fewer decoherence channels and less leakage. However, a recent experiment used a bias pulsing scheme.¹¹

Our system's Hilbert space is two-dimensional by construction [see Eq. (2)], hence there is no leakage to states outside the computational basis. We can, therefore, use square pulses instead of smooth, adiabatic ones. This not only allows us to analytically solve for the time evolution of the reduced density matrix, Eq. (8), but also renders our results applicable to both tunnel and bias pulsing. Indeed, in both regimes one has $\varepsilon(t) = 0$ and $v(t) = v_m$ for $t > 0$, taking that the pulse starts at $t = 0$. Let us assume that the excess electron is initially in the left dot: $\rho_{11}(0) = 1$ and $\rho_{12}(0) = 0$. In this case, since the coefficients on the right-hand side of (8) are all constants at $t > 0$, we can solve the Redfield equation exactly (see Appendix A for details). As $\rho(t)$ has only three real independent components, the solution is

$$\rho_{11}(t) = \frac{1}{2} + \frac{1}{2} e^{-\frac{\gamma_1}{2} t} (\cos \omega t + \frac{\gamma_1}{2\omega} \sin \omega t), \quad (18)$$

$$\text{Re } \rho_{12}(t) = -\frac{1}{2} (1 - e^{-\gamma_1 t}) \tanh \frac{v_m}{T}, \quad (19)$$

$$\text{Im } \rho_{12}(t) = \frac{2v_m + \gamma_2}{2\omega} e^{-\frac{\gamma_1}{2} t} \sin \omega t, \quad (20)$$

where

$$\omega = \left[4v_m \left(v_m + \frac{\gamma_2}{2}\right) - \frac{\gamma_1^2}{4}\right]^{1/2}, \quad (21)$$

$$\gamma_1 = \frac{\pi}{2} \nu(2v_m) \coth \frac{v_m}{T}, \quad (22)$$

$$\gamma_2 = -\int_0^\infty \frac{dy}{y^2 - 1} \nu(2v_m y) \coth \frac{v_m y}{T}. \quad (23)$$

Note that $\gamma_{1,2} \ll v_m$. We extract the customary energy and phase relaxation times, T_1 and T_2 , by rotating to the energy eigenbasis $\{|-\rangle, |+\rangle\}$:

$$\rho_{--}(t) = \frac{1}{2} - \text{Re } \rho_{12}(t), \quad (24)$$

$$\rho_{-+}(t) = -\frac{1}{2} + \rho_{11}(t) + i \text{Im } \rho_{12}(t). \quad (25)$$

Then, the damping of the oscillations in the diagonal matrix elements is the signature of energy relaxation, while the phonon-induced decoherence is seen in the exponential decay of the off-diagonal elements. For the DQD, we find $T_1 = \gamma_1^{-1}$ and $T_2 = 2\gamma_1^{-1}$ for the decoherence time.

The quality factor of the charge oscillations in Eq. (18) is $Q = \omega/\pi\gamma_1$. Using Eqs. (21), (22), and (15), we find that

$$Q \approx \frac{4 \tanh(v_m/T)}{\pi^2 g_{\text{ph}}} \left\{ \int_0^1 \frac{dx}{\sqrt{1-x}} e^{-(v_m/\omega_a)^2 x} \left[1 - J_0 \left(\frac{d}{a} \frac{v_m}{\omega_a} \sqrt{x} \right) \right] \right\}^{-1}, \quad (26)$$

where $\omega_a = s/2a$. The Q -factor depends on the tunneling amplitude v_m , lattice temperature T , dot radius a , and interdot distance d .

Several experimental realizations of DQD systems recently appeared in the literature.^{11,12,18,19} In principle, all these setups could be driven by tunnel pulsing to manipulate charge and perform single-qubit operations. To understand how the Q -factor depends on the tunneling amplitude v_m in realistic conditions, let us consider the DQD setup of Jeong and coworkers.¹⁸ In their device, each dot holds about 40 electrons and has a lithographic diameter of 180 nm. The effective radius a is estimated to be around 60 nm based on the device electron density. Therefore, $d/a \approx 3$. The lattice base temperature is 15 mK. Introducing these parameters into Eq. (26), one can plot Q -factor as a function of v_m or, equivalently, as a function of the period of the charge oscillations $P = 2\pi/\omega \approx \pi/v_m$. This is shown in Fig. 3.

To stay in the tunnel regime v_m should be smaller than the mean level spacing of each QD, approximately 400 μeV in the experiment.¹⁸ Therefore, in Fig. 3 we only show the curve for v_m up to 100 μeV . One has to recall that at these values the Markov approximation used in the Redfield formulation is not accurate (see end of Sec. II), and so our results are only an estimate for Q . For strong tunneling amplitudes, when $25 \mu\text{eV} < v_m < 100 \mu\text{eV}$, the largest value we find for Q is close to 100. For weak tunneling with $v_m < 25 \mu\text{eV}$, the situation is more favorable and larger quality factors (thus relatively less decoherence) can be achieved. Nevertheless, the one-qubit operation time, which is proportional to the period,

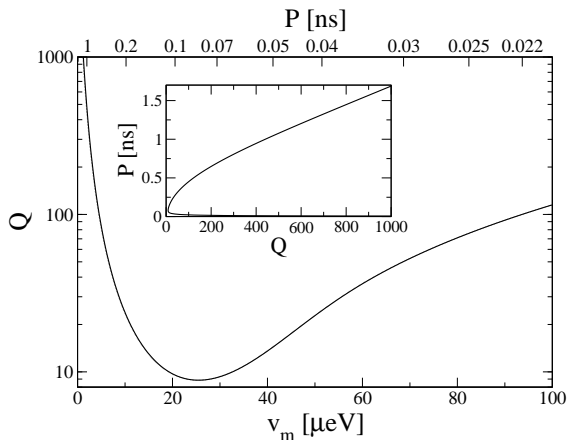


FIG. 3: The charge oscillation Q -factor as a function of the tunneling amplitude v_m (lower scale) and of the oscillation period P (upper scale) for a GaAs double quantum dot system. The lattice temperature is 15 mK and the dot radius and interdot distance are 60 nm and 180 nm, respectively. The inset shows the relation between P and Q at small tunneling amplitudes (large periods).

grows linearly with Q in the region of $v_m \rightarrow 0$, as shown in the inset of Fig. 3. Therefore, at a certain point other decoherence mechanisms are going to impose an upper bound on Q .

The minimum of Q in Fig. 3 occurs when v_m coincides with the frequency at which the phonon spectral density is maximum. It corresponds to the energy splitting between bonding and anti-bonding states of the DQD, $2v_m$, being approximately equal to the frequency of the strongest phonon mode s/a : $v_m \simeq \omega_a$.

From Fig. 3, it is evident that one can reach certain values for the Q -factor (say, $Q = 100$) at both weak ($v_m \simeq 4.6 \mu\text{eV} \simeq 53 \text{ mK}$) and strong ($v_m \simeq 93 \mu\text{eV} \simeq 1.1 \text{ K}$) tunneling. However, these two regimes are not equally convenient. From Eq. (26), it is clear that the temperature dependence of the Q -factor is fully determined by the bonding-antibonding splitting energy $2v_m$: $Q(T) = Q(0) \tanh(v_m/T)$. We notice that $Q(T) \approx Q(0)$ if $T \ll v_m$; therefore, the Q -factor is less susceptible to temperature variations for strong tunneling (Fig. 4). Another parameter that influences the Q -factor is the dot radius, which controls the frequency of the strongest phonon mode, s/a . In the strong tunneling regime (dashed curve in the inset to Fig. 4), one has to increase the QD size to improve the Q -factor. This would reduce the energy level spacing, hence only moderate improvement in Q -factor is possible. In contrast, in the weak tunneling regime (solid curve in the inset to Fig. 4) one has to reduce the QD size. This can lead to a significant (up to one order of magnitude) Q -factor improvement.

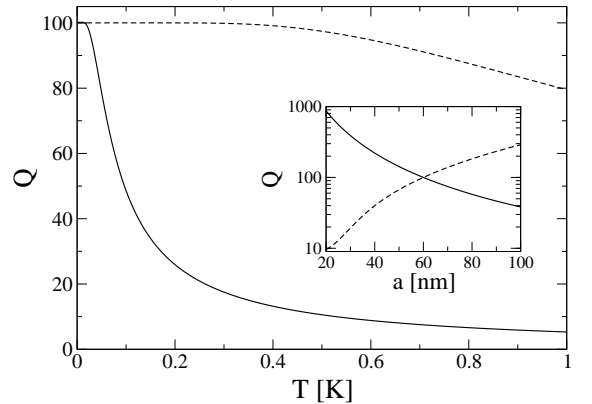


FIG. 4: The charge oscillation Q -factor as a function of the lattice temperature. Inset: as a function of the dot radius for a fixed ratio $d/a = 3$. The solid (dashed) line corresponds to the weak ($v_m \simeq 53 \text{ mK}$) (strong $v_m \simeq 1.1 \text{ K}$) tunneling regime. Other parameter values are equal to those in Fig. 3.

IV. BIAS PULSING

In a recent experiment,¹¹ Hayashi and coworkers studied charge oscillations in a bias-pulsed DQD. In this regime the energy difference between the left and right-dot single-particle energy levels is a function of time: $\varepsilon(t) = \varepsilon_0 u(t)$. A typical profile used for pulsing is

$$u(t) = 1 - \frac{1}{2} \left(\tanh \frac{t + W/2}{2\tau} - \tanh \frac{t - W/2}{2\tau} \right), \quad (27)$$

where W represents the pulse width and τ controls the rise and drop times. During bias pulsing, the tunneling amplitude is kept constant. In Ref. 11, the difference in energy levels was induced by applying a bias voltage between left and right leads (and not by gating the dots separately). For their setup, the maximum level splitting amplitude was $\varepsilon_0 \approx 30 \mu\text{eV}$ and $\tau \approx 15$ ps, corresponding to an effective ramping time of about 100 ps.²⁰ The tunneling amplitude was kept constant and estimated as $v \approx 5 \mu\text{eV}$, which amounts to charge oscillations with period $P \approx 1$ ns. The lattice temperature was 20 mK. Each quantum dot contained about 25 electrons and the effective dot radius is estimated to be around 50 nm based on the device electron density. From the electron micrograph of the device one finds $d \approx 225$ nm, hence $d/a \approx 4.5$. When substituting these values into Eq. (26), one finds $Q \approx 54$.

However, from the experimental data one observes $Q \approx 3$. Low Q -factors were also obtained by Petta and coworkers in an experiment where coherent charge oscillations in a DQD were detected upon exciting the system with microwave radiation.¹² Other mechanisms of decoherence do exist in these systems, such as background charge fluctuations²¹ and electromagnetic noise emerging from the gate voltages. Our results combined with the recent experiments indicate that these other mechanisms are more relevant than phonons.

We now turn to yet another possible source of decoherence: Leakage to the leads when the pulse is on.²² To illustrate this alternative source of damping of charge oscillations, we simulate the bias-pulsing experiment of Ref. 11 by implementing a rate equation formalism similar to that used in Ref. 23. The formalism is based on a transport theory put forward for the strongly biased limit.^{24,25} First, we find the stationary current I_0 through the DQD structure when the pulse is off (that is, the bias is applied):²⁵

$$I_0 = e \frac{\Gamma_L \Gamma_R}{\Gamma_L + \Gamma_R} \frac{v^2}{v^2 + \frac{\Gamma_L \Gamma_R}{4} + \frac{\varepsilon_0^2 \Gamma_L \Gamma_R}{(\Gamma_L + \Gamma_R)^2}}, \quad (28)$$

where e is the elementary charge. $\Gamma_{L(R)}$ is the partial width of the energy level in the left (right) dot due to coupling to the left (right) lead (when the bias is applied); in the experiment,¹¹ $\Gamma_{L,R} \approx 30 \mu\text{eV}$. On the other hand, when the pulse is on, the stationary current is zero. We now apply the pulse $\varepsilon(t)$ and measure the current $I(t)$. In the experiments, the level widths $\Gamma_{L,R}$ decrease upon biasing the system. To include that effect here, we also pulse them: $\Gamma_L(t) = \gamma_L + (\Gamma_L - \gamma_L)u(t)$ and analogously for Γ_R , where $\gamma_{L(R)}$ is the residual leakage to the left (right) lead when the pulse is on. We use $\gamma_{L,R} = 0.3 \mu\text{eV}$,

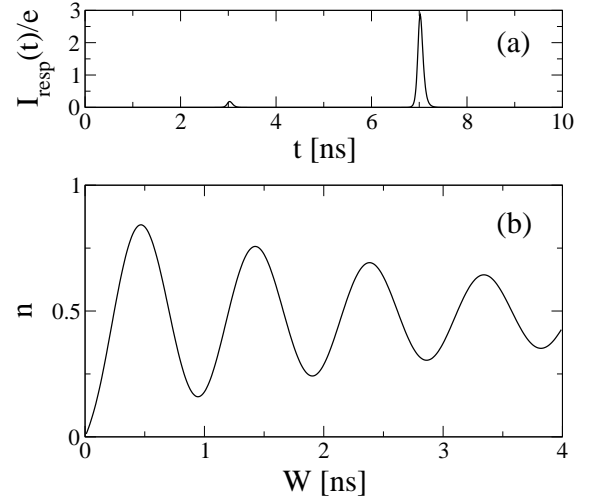


FIG. 5: (a) The response current $I_{\text{resp}}(t)/e$ in ns^{-1} as a function of time for a pulse with $W = 4$ ns and $\tau = 30$ ps. (b) Number of electrons transferred between left and right leads, as defined in Eq. (29), as a function of the pulse width W .

even though the real leakage in the experiment was likely much smaller. To obtain the response current one subtracts the stationary component: $I_{\text{resp}}(t) = I(t) - I_0 u(t)$.

Figure 5(a) shows the response current for a pulse of width $W = 4$ ns and $\tau = 30$ ps. The latter is approximately twice as large as in the experiment and is chosen to enhance the effect. In Ref. 11, pulses were applied at a frequency $f = 100$ MHz. The average number of electrons transferred from the left to the right lead per cycle minus that in the stationary regime is²³

$$n = \int_0^{1/f} dt I_{\text{resp}}(t)/e. \quad (29)$$

(In the simulations there is no need to apply a sequence of pulses.) Notice that n oscillates as a function of the pulse width W [see Fig. 5(b)] as observed in the experiment. Two main conclusions can be drawn from our simulation. First, the larger τ , the smaller the visibility of the charge oscillations.²³ Second, the larger the leakage rates $\gamma_{L,R}$ when the pulse is on, the stronger the damping of the oscillations. While the damping due to leakage is presumably too weak an effect to discern in the data presented in Ref. 11, the loss of visibility due to finite τ is likely one of the causes of the small amplitude seen experimentally.

V. CONCLUSIONS

The main conclusion of the paper is that, under realistic conditions, phonon decoherence is one to two orders of magnitude weaker than expected.^{6,7,8} The analytical expression for the Q -factor given in Eq. (26) was found using an expression for the phonon spectral density, Eq. (15), which takes into account important information concerning the geometry of the double quantum dot system. In a previous work⁷ an approximate, phenomenological expression, $\nu(\omega) \propto \omega \exp(-\omega/\omega_c)$, was utilized in the treatment of charge qubits. There is a

striking difference between these two expressions in both the high- and low-frequency limits. Moreover, an arbitrary coupling constant was adopted in Ref. 7 to model the electron-phonon interaction while our treatment uses a value known to describe the most relevant phonon coupling in GaAs. On the other hand, other previous work^{6,8} assumed a spherically symmetric excess charge distribution in the dot while we have assumed a two-dimensional pancake form. These differences account for most of the discrepancy between the present and previous results.

Based on these findings we conclude that phonon decoherence is too weak to explain the damping of the charge oscillations seen in recent experiments.^{11,12} Charge leakage to the leads during bias pulsing is an additional source of damping, as shown in Fig. 5(b); however, for realistic parameters,^{11,23} it turns out to be a weak effect as well. Hence, other decoherence mechanisms, such as background charge fluctuations or noise in the gate voltages, play the dominant role.²¹

There are two distinct ways to operate a double quantum dot charge qubit: (i) by tunnel pulsing or (ii) by bias pulsing. Tunnel pulsing seems advantageous due to the smaller number of possible decoherence channels. In addition, the bias pulsing scheme, in contrast to tunnel pulsing, introduces significant loss of visibility in the charge oscillations.

In this work we did not attempt to study leakage or loss of fidelity due to non-adiabatic pulsing, which are both important issues for *spin*-based quantum dot qubits.²⁶ Moreover, we have not attempted to go beyond the Markov approximation when deriving an equation of motion for the reduced density matrix. Both of these restrictions in our treatment impose some limitations on the accuracy of our results, especially for large tunneling amplitudes.

Finally, it is worth mentioning that some extra insight would be gained by measuring the Q -factor as a function of the tunneling amplitude v_m experimentally. Such a measurement would allow one to map the spectral density of the boson modes responsible for the decoherence. This would provide very valuable information about the leading decoherence mechanisms in double quantum dot systems.

Acknowledgments

We thank A. M. Chang, M. Hentschel, E. Novais, G. Usaj, and F. K. Wilhelm for useful discussions. This work was supported in part by the National Security Agency and the Advanced Research and Development Activity under ARO contract DAAD19-02-1-0079. Partial support in Brazil was provided by Instituto do Milênio de Nanociência, CNPq,

FAPERJ, and PRONEX.

APPENDIX A: DERIVATION OF EQS. (18), (19), AND (20)

For $t > 0$, Eq. (2) is time-independent: $H_S = v_m \sigma_x$. Since the K matrix is also time-independent [Eq. (7)], the matrix Λ defined by Eq. (9) is time-independent as well. After some straightforward operator algebra, we find that

$$\Lambda = \frac{1}{2} \int_0^\infty d\tau B(\tau) e^{-i\tau v_m \sigma_x} \sigma_z e^{i\tau v_m \sigma_x} \quad (\text{A1})$$

$$= \frac{1}{2} \int_0^\infty d\tau B(\tau) [\sigma_z \cos(2v_m \tau) - \sigma_y \sin(2v_m \tau)]. \quad (\text{A2})$$

One can rewrite Eq. (A2) as follows

$$\Lambda = \frac{1}{2}(\gamma_1 + i\gamma_3)\sigma_z - \frac{1}{2}(\gamma_2 + i\gamma_4)\sigma_y, \quad (\text{A3})$$

where $\{\gamma_i\}$'s are real coefficients:

$$\begin{Bmatrix} \gamma_1 + i\gamma_3 \\ \gamma_2 + i\gamma_4 \end{Bmatrix} = \int_0^\infty d\tau B(\tau) \begin{Bmatrix} \cos(2v_m \tau) \\ \sin(2v_m \tau) \end{Bmatrix}. \quad (\text{A4})$$

The density matrix $\rho(t)$ is a 2×2 Hermitian matrix with unit trace. Hence, it has three real independent components and can be written as follows:

$$\rho = \frac{1}{2} + \sigma_x \text{Re } \rho_{12} - \sigma_y \text{Im } \rho_{12} + \sigma_z (\rho_{11} - \frac{1}{2}). \quad (\text{A5})$$

Let us substitute Eqs. (A5) and (A3) into the Redfield equation [Eq. (8)] and use that $H_S = v_m \sigma_x$ and $K = \frac{1}{2} \sigma_z$. A simple algebraic manipulation leads to three differential equations,

$$\text{Re } \dot{\rho}_{12} = -\gamma_1 \text{Re } \rho_{12} + \frac{\gamma_4}{2}, \quad (\text{A6})$$

$$\dot{\rho}_{11} = -2v_m \text{Im } \rho_{12}, \quad (\text{A7})$$

$$\text{Im } \dot{\rho}_{12} = (2v_m + \gamma_2)(\rho_{11} - \frac{1}{2}) - \gamma_1 \text{Im } \rho_{12}. \quad (\text{A8})$$

The initial conditions are $\rho_{11}(0) = 1$ and $\rho_{12}(0) = 0$. Eq. (A6) decouples from Eqs. (A7) and (A8). Its solution is given by Eq. (19), where we used the following identity: $\gamma_4/\gamma_1 = -\tanh(v_m/T)$. Eqs. (A7) and (A8) form a closed system. Their solution is given by Eqs. (18) and (20).

The coefficients γ_1 and γ_2 [Eqs. (22) and (23), respectively] are calculated using Eqs. (A4) and (10).

¹ M. A. Nielsen and I. L. Chuang, *Quantum Computation and Quantum Information* (Cambridge University Press, Cambridge, U.K., 2000).

² D. Loss and D. P. DiVincenzo, Phys. Rev. A **57**, 120 (1998).

³ D. P. DiVincenzo, D. Bacon, J. Kempe, G. Burkard, and K. B. Whaley, Nature **408**, 339 (2000).

⁴ R. H. Blick and H. Lorenz, in Proceedings of the IEEE International Symposium on Circuits and Systems, edited by J. Calder (IEEE, Piscataway, NJ, 2000), Vol. II, p. 245.

⁵ T. Tanamoto, Phys. Rev. A **61**, 022305 (2000).

⁶ L. Fedichkin and A. Fedorov, Phys. Rev. A **69**, 032311 (2004); L. Fedichkin, M. Yanchenko, and K. A. Valiev, Nanotechnology

- 11**, 387 (2000).
- ⁷ T. Brandes and T. Vorrath, Phys. Rev. B **66**, 075341 (2002).
 - ⁸ Z.-J. Wu, K.-D. Zhu, X.-Z. Yuan, Y.-W. Jiang, and H. Zheng, preprint cond-mat/0412503.
 - ⁹ D. P. DiVincenzo, G. Burkard, D. Loss, and E. V. Sukhorukov, in *Quantum Mesoscopic Phenomena and Mesoscopic Devices in Microelectronics*, edited by I. O. Kulik and R. Ellialtıoğlu (Kluwer, 2000), cond-mat/9911245.
 - ¹⁰ W. G. van der Wiel, S. De Franceschi, J. M. Elzerman, T. Fujisawa, S. Tarucha, and L. P. Kouwenhoven, Rev. Mod. Phys. **75**, 1 (2003).
 - ¹¹ T. Hayashi, T. Fujisawa, H. D. Cheong, Y. H. Jeong, and Y. Hirayama, Phys. Rev. Lett. **91**, 226804 (2003); T. Fujisawa, T. Hayashi, H. D. Cheong, Y. H. Jeong, and Y. Hirayama, Physica E **21**, 1046 (2004).
 - ¹² J. R. Petta, A. C. Johnson, C. M. Marcus, M. P. Hanson, and A. C. Gossard, Phys. Rev. Lett. **93**, 186802 (2004).
 - ¹³ P. N. Argyres and P. L. Kelley, Phys. Rev. **134**, A98 (1964).
 - ¹⁴ W. T. Pollard and R. A. Friesner, J. Chem. Phys. **100**, 5054 (1994).
 - ¹⁵ In the situation we envision, the total number of electrons would be odd: The ground state of each dot in the absence of the excess electron would have $S=0$, so that the dot with the excess electron would have spin half. Other situations are, of course, possible, such as the total number of electrons being even with $S=0$ for both dots when the qubit is in state $|1\rangle$ and $S=1/2$ for both in state $|2\rangle$; in the latter case, there would be a singlet and triplet state of the DQD with a small exchange splitting. Such complications do not effect the underlying physics that we discuss, and so we neglect them.
 - ¹⁶ T. Brandes and B. Kramer, Phys. Rev. Lett. **83**, 3021 (1999).
 - ¹⁷ H. Bruus, K. Flensberg, and H. Smith, Phys. Rev. B **48**, 11144 (1993).
 - ¹⁸ H. Jeong, A. M. Chang, and M. R. Melloch, Science **293**, 2221 (2001).
 - ¹⁹ J. C. Chen, A. M. Chang, and M. R. Melloch, Phys. Rev. Lett. **92**, 176801 (2004).
 - ²⁰ The value of $\tau \approx 15$ ps is obtained by fitting Eq. (27) to the experimental pulse with an effective ramping time of 100 ps, Ref. 23.
 - ²¹ T. Itakura and Y. Tokura, Phys. Rev. B **67**, 195320 (2003).
 - ²² For another source of decoherence due to coupling to the leads, see U. Hartmann and F. K. Wilhelm, Phys. Rev. B **69**, 161309(R) (2004).
 - ²³ T. Fujisawa, T. Hayashi, and Y. Hirayama, J. Vac. Sci. Technol. B **22**, 2035 (2004).
 - ²⁴ Yu. V. Nazarov, Physica B **189**, 57 (1993).
 - ²⁵ S. A. Gurvitz and Ya. S. Prager, Phys. Rev. B **53**, 15932 (1996).
 - ²⁶ S. Vorojtsov, E. R. Mucciolo, and H. U. Baranger, Phys. Rev. B **69**, 115329 (2004).